Transient Flow Field in Containment Floor Following a LOCA of APR-1400

Young Seok Bang [a*], Gil-Soo Lee [a], Byung-Gil Huh [a], Deog-Yeon Oh [a], and Sweng Woong Woo [a]
[a] *Korea Institute of Nuclear Safety, 19 Gusung-Dong, Yuseong-Gu, Daejeon, 305-335, Korea*
[*] *Corresponding author: k164bys@kins.re.kr*

1. Introduction

Adoption of In-containment Refueling Water Storage Tank (IRWST) in APR(Advanced Power Reactor)-1400 effectively removed the switchover process for water source of emergency core cooling system (ECCS) and containment spray system following a Loss-of-Coolant Accident (LOCA) [1]. However, it may impose an additional challenge for the resolution of the sump clogging issue (GSI-191) [2] because the containment flow field should be calculated in "transient" instead of "steady" since the flow paths from the break location to containment sump may be established at the early phase of the LOCA.

The present study is to discuss an analysis model to calculate the transient flow field on containment floor to be used debris transport. The model has been developed to overcome the weaknesses in existing calculation method, i.e, non-physical modeling and high uncertainty when using a system transient code such as RELAP5 and long computational time in Computational Fluid Dynamics (CFD) code.

2. Analysis Model

The governing equation of the present model is shallow water equation (SWE) which can be derived from Navier Stokes equation with assumption of vertically uniform flow and free surface formula [3]:

$$\frac{\partial \boldsymbol{W}}{\partial t}+\frac{\partial \boldsymbol{F}}{\partial x}+\frac{\partial \boldsymbol{G}}{\partial y}=\frac{\partial \boldsymbol{R}_x}{\partial x}+\frac{\partial \boldsymbol{R}_y}{\partial y}+\boldsymbol{S} \quad \text{.......}(1)$$

$$\begin{aligned}
&\boldsymbol{W}=[h, hu, hv]^T,\ \boldsymbol{F}=[hu, hu^2+1/2gh^2, huv]^T,\\
&\boldsymbol{G}=[hv, huv, hv^2+1/2gh^2]^T \qquad \text{.......}(2)\\
&\boldsymbol{R_x}=[0, \nu_t(\partial hu/\partial x), \nu_t(\partial hv/\partial x)]^T,\\
&\boldsymbol{R_y}=[0, \nu_t(\partial hu/\partial y), \nu_t(\partial hv/\partial y)]^T\\
&\boldsymbol{S}=[B, -\partial z_b/\partial x - gn^2uq, -\partial z_b/\partial y - gn^2vq]^T\\
&q=\sqrt{u^2+v^2}/h^{1/3}
\end{aligned}$$

Eq.(1) is integrated for a cell V surrounded C, then,

$$\int_V \frac{\partial \boldsymbol{W}}{\partial t}dv+\int_C(\boldsymbol{F}n_x+\boldsymbol{G}n_y)dC=\int_C(\boldsymbol{R}_x n_x+\boldsymbol{R}_y n_y)dC+\int_V \boldsymbol{S}dv \quad \text{........}(3)$$

The finite volume equation of the Eq.(3) for a triangular mesh can be written as follows:

$$A_k\frac{d\boldsymbol{W}_k}{dt}+\sum_{j=1}^{3}\{\boldsymbol{F}_{kj}L_{xj}+\boldsymbol{G}_{kj}L_{yj}\}=\sum_{j=1}^{3}\{\boldsymbol{R}_{x,kj}L_{xj}+\boldsymbol{R}_{y,kj}L_{yj}\}+A_k\boldsymbol{S}_k \quad \text{........}(4)$$

Eq.(4) is solved at the center of all the cells using the fluxes across the cell sides. In order to preserve the second order accuracy, the predictor-corrector scheme was used.

$$\begin{aligned}
&\boldsymbol{W}_k^{n+1/2}=\boldsymbol{W}_k^n-\frac{\Delta t}{2A_k}\sum_{j=1}^{3}Flux_{conv}^n+\frac{\Delta t}{2A_k}\sum_{j=1}^{3}Flux_{diffus}^n+\frac{\Delta t}{2}\boldsymbol{S}_k^{\ n} \quad \text{......}(5)\\
&\boldsymbol{W}_k^{n+1}=\boldsymbol{W}_k^n-\frac{\Delta t}{A_k}\sum_{j=1}^{3}Flux^{*n+1/2}_{conv}+\frac{\Delta t}{A_k}\sum_{j=1}^{3}Flux_{diffus}^{n+1/2}+\Delta t\boldsymbol{S}_k^{\ n}
\end{aligned}$$

An approximate Riemann solver, Harten-Lax-van Leer (HLL) scheme [4] was implemented to the corrector step, to avoid unphysical oscillation and instability of the solution especially at the wet-dry interface.

$$F^*(U_R,U_L)=\frac{[(s_R\boldsymbol{F}(U_L)-s_L\boldsymbol{F}(U_R))\cdot\boldsymbol{n}+s_Ls_R(U_R-U_L)]}{s_R-s_L} \quad \text{.....}(6)$$

$$\begin{aligned}
&s_L=\min(\boldsymbol{q}(U_L)\cdot\boldsymbol{n}-c(h_L),\ \boldsymbol{q}^*\cdot\boldsymbol{n}-c^*), \qquad \text{.......................}(7)\\
&s_R=\max(\boldsymbol{q}(U_R)\cdot\boldsymbol{n}-c(h_R),\ \boldsymbol{q}^*\cdot\boldsymbol{n}+c^*)\\
&\boldsymbol{q}(U)=(u,v),\ \ c(h)=\sqrt{gh},\\
&\boldsymbol{q}^*\cdot\boldsymbol{n}=\frac{1}{2}(\boldsymbol{q}(U_L)+\boldsymbol{q}(U_R))\cdot\boldsymbol{n}+c(h_L)-c(h_R),\\
&c^*=\frac{1}{2}(c(h_L)+c(h_R))+\frac{1}{4}(\boldsymbol{q}(U_L)-\boldsymbol{q}(U_R))\cdot\boldsymbol{n}
\end{aligned}$$

The diffusive flux term (third one of RHS of Eq.(5)) was approximated by the central difference scheme. The source term also can be approximated in cell area-weighted basis. The time step size to solve the Eq.(5) should be limited to prevent the negative water level as follow [3]:

$$\Delta t \le Min_k\left(\frac{A_k}{K_{CFL}Max|\boldsymbol{q}(U)\cdot\boldsymbol{n}\pm c|_{kj}}\right) \quad \text{.................................}(8)$$

K_{CFL} is a coefficient similar to the Courant-Fredrich-Lewy (CFL) number in CFD calculation and set to 1.3.

3. Model Verification

To support the validity of the present model, the experiment [5] was calculated by the present model. Fig. 1 shows a schematic representation of the experiment. The reservoir was initially filled with water by 0.2 m and a L-shaped open channel was connected in dry state. A gate in front of the pool was instantaneously ruptured. Water level was measured at several locations as in Fig. 1. The experiment system was simulated by 2231computational cells. At the exit of the L-shaped channel, the Neumann-type open boundary condition was imposed and no-slip condition was imposed at all wall boundaries.

Fig. 2 shows the calculated water level at the points P3. As shown in those figures, the calculated behaviour of water level was well agreed to the measured data. It can be stated, accordingly, the validity and accuracy of the present model were fully justified.

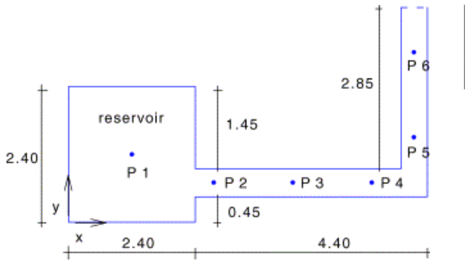

Fig. 1 Experimental Setup

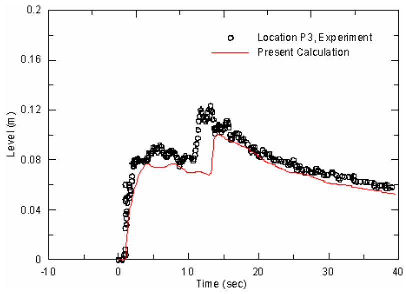

Fig. 2 Comparison of Water Level at P3

4. Application to APR-1400

The containment floor of APR-1400 was modeled by 4792 cells as shown in Fig 3. As a boundary condition, no slip condition ($u=v=0$) is imposed for the solid wall. Water level at wall is assumed to be the same as the one at the center of the adjacent cell. At the entrance to HVT pit, the analytic model of the discharge flow rate at the broad crested weir [6] was used. The calculation was carried until 200 seconds. Fig. 4 shows the typical result of the calculation, local water level and velocity vector at 5 seconds following a LOCA. Fig. 5 shows flow rates at four entrance lines to HVT. Total CPU time was 18000 sec in Pentium 4, 3.4 GHz processor.

3. Concluding Remarks

Two-dimensional shallow water equation in finite volume method was solved with unstructured triangular meshes for the transient flow field in containment floor following a LOCA. The Harten-Lax-van Leer scheme was used to calculate the flux term at cell-to-cell interface where bed wetting and drying are present. The model was verified with the experimental data. The transient flow field on containment floor of APR-1400 was calculated, thus, it can be concluded that the model has a validity and performance sufficient to be used in the debris transport analysis.

REFERENCES

[1] KEPCO, Standard Safety Analysis Report, Advanced Power Reactor 1400, 1992

[2] USNRC, Regulatory Guide 1.82, Revision 3, “Water Sources for Long-Term Recirculation Cooling Following a Loss-of-Coolant Accident,” 2003

[3] L. Begnudelli, B.F. Sanders, “Unstructured Grid Finite-Volume Algorithm for Shallow-Water Flow and Scalar Transport with Wetting and Drying”, ASCE Journal of Hydraulic Engineering, Vol. 132, No. 4, 2006

[4] A. Harten, P.D. Lax B. van Leer, “On Upstream Differencing and Godunov-Type Schemes for Hyperbolic Conservation Laws”, SIAM Rev. 25, pp 35–61, 1983

[5] Brufau P, Garcia-Navarro P. “Two-dimensional dam break flow simulation”, International Journal of Numerical Method in Fluids, Vol. 33, pp 35–57, 2000

[6] ANS, Design Criteria for Protection against the Effects of Compartment Flooding in Light Water Reactor Plants, ANSI/ANS-56.11, 1988.

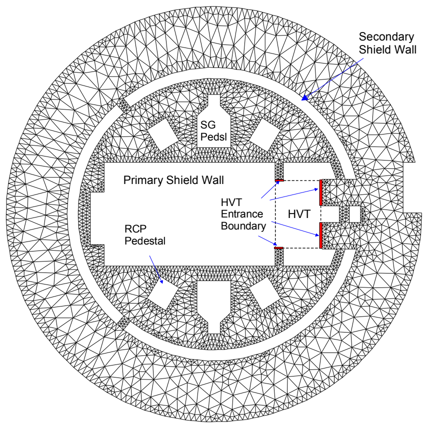

Fig. 3. Mesh System of Containment floor of APR-1400

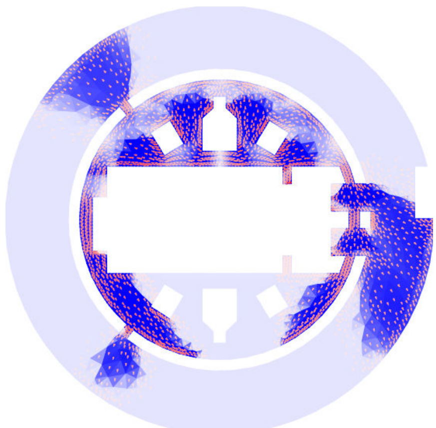

Fig. 4 Flow Field at 5 sec after LOCA

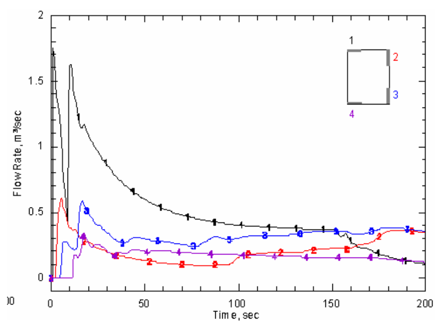

Fig. 5 Flow Rates at HVT Entrance